Quaternary Science Reviews 338 (2024) 108820

Contents lists available at ScienceDirect

Quaternary Science Reviews

journal homepage: www.elsevier.com/locate/quascirev

Wildfire-vegetation-climate-human interactions in the central Taiwan region during 17.3–2.0 cal kyr BP, inferred from sediments of Toushe Basin

Abdur Rahman [a,b], Yuan-Pin Chang [c,d], Hong-Chun Li [e], Ling-Ho Chung [f,g], Yu-Min Chou [h], Liang-Chi Wang [a,b,*]

[a] Department of Earth and Environmental Sciences, National Chung Cheng University, Chiayi, 621, Taiwan
[b] Environment and Disaster Monitoring Center, National Chung Cheng University, Chiayi, 621, Taiwan
[c] Department of Oceanography, National Sun Yat-sen University, Kaohsiung, 804, Taiwan
[d] Sustainable Ocean Governance Center, National Sun Yat-sen University, Kaohsiung, 804, Taiwan
[e] Department of Geosciences, National Taiwan University, Taipei, 106, Taiwan
[f] National Museum of Natural Science, Taichung, 404, Taiwan
[g] Center for General Education, National Chung Cheng University, Chiayi, 621, Taiwan
[h] Department of Ocean Science and Engineering, Southern University of Science and Technology, Shenzhen, 518055, PR China

ARTICLE INFO

Handling Editor: P Rioual

Keywords:
Wildfire
Charcoal
Taiwan climate
Stable isotope
Human activities

ABSTRACT

In this study, a long-term relationship amongst wildfire, vegetation, climate, and human in the central Taiwan region, spanning from 17.3 to 2.0 cal kyr BP, is explored. To investigate this relationship, multiple proxy approaches were employed, including charcoal (CHAR and fire frequency), pollen data (Liew et al., 2006), magnetic susceptibility, and the carbon isotopic composition of organic carbon, along with the elemental ratio of total organic carbon to total nitrogen in the core sediments of the Toushe Basin, central Taiwan. From 17.3 to 14.5 cal kyr BP, the Toushe Basin experienced drier climate conditions, leading to high-intensity fires and reduced area of wetland. Between 14.5 and 11.5 cal kyr BP, a wetter climate corresponded with low-intensity fires and an increase in tree prevalence. From 11.5 to 5.0 cal kyr BP, the climate remained relatively stable with peaks of extreme wet phases, with frequent low-intensity fires promoting herbaceous plant growth. During the period from 5.0 to 2.0 cal kyr BP, wetter conditions persisted, but increased human activities likely intensified high-intensity fires, resulting in reduced tree and herbaceous plant populations and an expansion of wetlands, leading to complex impacts on the region's ecological dynamics. The pollen diversity index (PDI) and pollen richness index (PRI) showed that ecological diversity in the Toushe Basin decreased with high-intensity fires and increased with low-intensity fires, highlighting the complex interactions between natural and human factors during 17.3–2.0 cal kyr BP. In addition, this study showed a strong link between El-Niño events and increased wildfire activity in the Toushe Basin. El-Niño conditions, with reduced rainfall and increased dryness, likely heightened wildfire frequencies and intensity by lowering moisture levels and ignition thresholds. Increased lightning during these periods further exacerbated wildfires. This connection highlights El-Niño 's role in driving high-intensity fires, impacting the region's vegetation and ecological dynamics.

1. Introduction

Wildfires create a significant disturbance in global forests, and their frequency is heavily influenced by climate (Dale et al., 2001; Laurance, 2004; Seidl et al., 2011). Recently, rising temperatures have changed the fire patterns in the Northern Hemisphere, causing more frequent and extreme wildfire seasons in forests (Kitzberger et al., 2001; Flannigan et al., 2013; Tao, 2024). As a result, the impact of wildfires on natural ecosystems, landscapes, and the global biogeochemical cycle has become more severe (Corona-Núñez et al., 2020; Magerl et al., 2023). This has led to many countries adopting stricter forest management and wildfire suppression policies. However, actively suppressing fires without considering the unique role of wildfires may increase tree density and the availability of biofuels, resulting in more wildfires (Archibald, 2016; Cochrane and Bowman, 2021; Hayes, 2021). To deepen our understanding of the mechanisms driving wildfires along

* Corresponding author. Department of Earth and Environmental Sciences, National Chung Cheng University, Chiayi, 621, Taiwan.
E-mail address: lcwang@ccu.edu.tw (L.-C. Wang).

https://doi.org/10.1016/j.quascirev.2024.108820
Received 30 March 2024; Received in revised form 19 June 2024; Accepted 2 July 2024
Available online 12 July 2024

with its relation with vegetation, it is essential to examine the frequency and origin of wildfires over a longer time scale than that of modern observations.

Previous records demonstrated that significant wildfires, both in recent times and throughout history, have occurred during periods of drier climates (Halofsky et al., 2020; Liu et al., 2010; Remy et al., 2023; Verma et al., 2023). Projections suggest that ongoing global changes will likely intensify these dry phases, resulting in unusual fire events (Barbero et al., 2015). This is because the increase in precipitation will not sufficiently counter the heightened evaporation due to rising temperatures (Ji et al., 2021; Yuan et al., 2022; Remy et al., 2023). Periodic dry events linked to El-Niño events and other supra-annual climate variability may also heighten the likelihood of fires (Harrison and Meindl, 2001; Letnic et al., 2005; Huang et al., 2020). During severe dry conditions, wildfires can spread into forests where fires are relatively uncommon (Ruffault et al., 2018; Stephens et al., 2018). In addition to appropriate climate and biofuels, a wildfire necessitates an ignition source (Syphard and Keeley, 2015; Ganteaume and Syphard, 2018). Dry lightning has historically been a significant ignition source across numerous biomes (Klenner et al., 2008; Ganteaume and Syphard, 2018). Later, human replaced the ignition source of fire and now is the primary source of ignition (Keeley and Syphard, 2018; Villarreal et al., 2022).

Additionally, along with climate, the relationship between vegetation and flammability at the species level is important for a broader understanding of the vegetation-fire dynamic at the local and landscape scales (Tumino et al., 2019; Popović et al., 2021). Wildfires are frequent and anticipated events in grasslands, savannas, Mediterranean shrublands, forests, and boreal forests (Prichard et al., 2017; Pausas and Keeley, 2021). They are also seen as a secondary factor influencing the distribution of vegetation (Hyde et al., 2016; Foster et al., 2017). It has been proposed that about 40% of the Earth's land surface is covered by vegetation that is prone to wildfires (Liu et al., 2022). These fires disrupt forests, leading to their transformation into shrublands or grasslands, depending on the fire's frequency and intensity (Lloret et al., 2002; Acácio et al., 2009). Overall, it seems there are two potential scenarios: (i) climate shifts influencing vegetation, thereby regulating wildfire activity (Jolly et al., 2015; Potera, 2009), and (ii) wildfires altering the vegetation type by disrupting forested areas (Certini, 2005; Walker et al., 2018). However, investigating this relationship on a longer time scale is quite challenging due to the limited availability of information regarding vegetation and wildfires.

Paleoecological studies endeavor to unravel the interaction between wildfire, vegetation, climate, and humans over extended time periods (Lin et al., 2023; Wang, 2021, 2024; Wang et al., 2020). Various proxies of vegetation (pollen and sedimentary DNA) and indicators of wildfires (charcoal, black carbon, polycyclic aromatic hydrocarbons) are utilized for this purpose (Rahman et al., 2021; Glückler et al., 2022; Remy et al., 2023; Verma et al., 2023). An investigation in the boreal forest of northern Fennoscandia exemplified the impact of climate on fire patterns (Remy et al., 2023). This study demonstrated that warm and dry periods were conducive to significant forest fires, while cool and wet periods were linked to smaller fires throughout the Holocene. In Central Yakutia, Siberia, a study utilizing charcoal and sedimentary DNA metabarcoding projected an increase in forest disturbances like wildfires and droughts, potentially leading to higher tree mortality and a shift in the modern forest towards an open woodland state similar to the conditions during early Holocene (Glückler et al., 2022). Many studies have endeavored to explore the interaction among wildfire, vegetation, climate, and humans in the Asian regions (Tan et al., 2013, 2015; Pang et al., 2021; Verma et al., 2023). Human-induced wildfires were widespread during the Holocene in Asia (Tan et al., 2013, 2015; Verma et al., 2023). Nonetheless, our comprehension of the relationship between vegetation and wildfires in the context of climate change is limited due to an insufficient amount of data. Consequently, conducting more in-depth studies over longer time periods is necessary to address this knowledge gap.

Taiwan, an island in the subtropical region, experiences a climate influenced by the East Asian Monsoon. It is characterized by warm and wet summers, coupled with cool and dry winters. Generally, Taiwan is known for its humid climate, which contributes to the island being covered by approximately 58% forested land. The present vegetation of Taiwan is dominated by subtropical evergreen forests. Studies classified the variety of vegetation types in the mountains of central Taiwan and identified different altitudinal zones along with their respective annual temperature ranges (Table S1). Taiwan has been thoroughly investigated in terms of pollen stratigraphy, shedding light on its paleovegetation diversity (Huang et al., 2020; Wang et al., 2019, 2020; Wang, 2021, 2024). In a recent study utilizing pollen and charcoal analysis, it was found that wildfires in central Taiwan were probably influenced by fluctuations in precipitation, driven by the East Asia Summer Monsoon and El-Niño–Southern Oscillation (Huang et al., 2020). Specifically, it has been mentioned that Toushe Basin experienced drought conditions and frequent wildfires during the El-Niño years throughout the mid to late Holocene. Furthermore, previous paleo wildfire studies in Taiwan have mainly focused on the mid to late Holocene period, emphasizing the relationship between wildfires and human activity (Wenske et al., 2011; Huang et al., 2020; Wang, 2021, 2024). In contrast, our study expands the scope to encompass the interaction between wildfires, vegetation, climate, and humans, beyond the late Holocene. We utilized charcoal, magnetic susceptibility and stable isotopes of total organic carbon in sediment from the Toushe Basin. Additionally, we incorporated the published pollen data from the same basin, provided by Liew et al. (2006), covering a similar timeframe to examine vegetation patterns and its relation with wildfires.

2. Material and methods

The Toushe Basin (23° 49′ N, 120° 53′ E), located in central Taiwan, is situated at an elevation of 642 m above sea level and covers an area of approximately 1.75 km^2 (Fig. 1). The watershed upstream of the Toushe Basin encompasses about 495 ha (Chen et al., 2009). No local meteorological data are available for the basin; however, data from the nearby Sun-Moon Lake station show that the mean annual rainfall and temperature of the area is 2300 mm and 21 °C, respectively. Overall, the area experiences a humid, subtropical, monsoonal climate with average temperatures in the warmest and coldest months of 25 °C and 14 °C, respectively. A 27-year timeline of monthly average temperature and precipitation is shown in Fig. 1d. The contemporary vegetation in the study area consists of subtropical evergreen forests dominated by the Lauro-Fagaceae family (Liew et al., 2006).

A 776 cm-long core (TS 19) was extracted from peatland in the Toushe Basin (23°49′41.5″ N, 120°54′11.9″ E) and subsampled at 2-cm intervals for reconstructing high resolution paleoclimate records (Fig. 1). Samples were oven-dried to remove moisture and then pulverized to a fine grain. Powdered samples of 0.1 g were put into centrifuge tubes and then treated with HCl to remove the inorganic fraction. The decarbonated samples were oven dried overnight. After drying, samples were packed into tin capsules and combusted in an Elemental Analyzer (EA, Flash, 2000; Thermo Fisher Scientific, Waltham, MA, USA) at 1020 °C, converting the organic matter into CO_2. The produced CO_2 was transferred to an isotope ratio mass spectrometer (Finnigan DELTAplus Advantage; Thermo Fisher Scientific) using He as a carrier gas. The carbon isotopic ratio ($\delta^{13}C$, expressed in per mil; ‰) of the organic sample and its C content were then measured. USGS 40 (NIST 8573) L-glutamic acid ($\delta^{13}C = -26.39 \pm 0.04$‰ and C content = 40.8%) was used to check instrument working conditions and precision. The analytical precision of $\delta^{13}C$ and C content in repeated samples were 0.1‰ and <10%, respectively. The N contents were measured at the same time as the C using the jump method in the EA.

The mass magnetic susceptibility (MS) of Toushe Basin sediments was measured on dry sub-samples using a Kappa bridge (MFK2-FA) at the Centre for Marine Magnetism (CM2), Southern University of Science

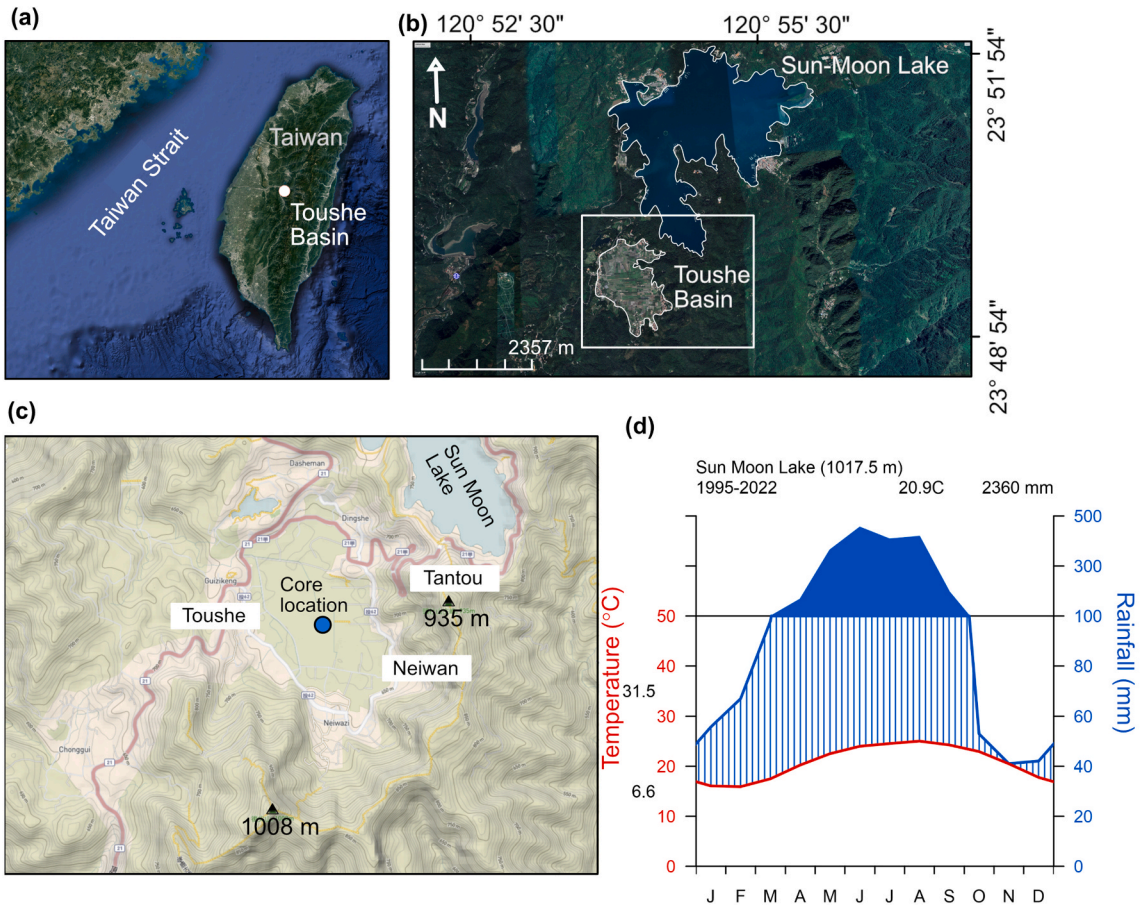

Fig. 1. (a) Map of Taiwan with a white dot indicating the location of the study area, Toushe Basin, (b) location of Toushe Basin (study area) and Sun-Moon Lake with approximate boundaries (white outlines), (c) topographic map of the Toushe Basin (source: Get Maps | topoView (usgs.gov)) and blue dot represents the location of core, and (d) Walter-Lieth climatic diagram of the 27-year monthly average of temperature and rainfall in the area of Sun-Moon Lake (obtained from the Central Weather Bureau, Taiwan). Compiled using the R package 'climatol' (Guijarro, 2019). Images were captured from Google Earth.

and Technology (SUSTech), Shenzhen, China.

To construct the chronology of the core, 21 organic matter samples from different depths were radiocarbon dated (Table 1). Radiocarbon dating was performed in the NTU-AMS lab in Taiwan. An age-depth model was constructed using Bayesian statistics and implemented using the package "rbacon" in R with the IntCal20 calibration curve (Blaauw et al., 2021; Reimer et al., 2020) (Fig. 2).

In the context of charcoal analysis, specimens measuring 2 cm^3 were subjected to a treatment process with 12% sodium hypochlorite (NaClO) for a period no less than two days. This procedure aimed at the elimination of organic constituents from the samples (Whitlock and Larsen, 2002). Following this initial treatment, the samples underwent a wet-sieving method using a mesh with a pore size of 125 μm, which facilitated the segregation of charcoal fragments. The marco-charcoal particles (pieces/cm^3) were counted under a stereomicroscope and the charcoal surface area (cm^2/cm^3) was calculated using the software ImageJ.

Reconstruction of wildfire history was performed by analyzing the charcoal data using Char-Analysis 1.1. code for MATLAB R2021 (Higuera et al., 2009). The charcoal counts data were interpolated to achieve a median temporal resolution of 34 years. Following this, a logarithmic transformation was applied to the interpolated data, enabling the evaluation of the charcoal accumulation rate (CHAR, delineated in pieces cm^2 yr^{-1}) in consistent temporal intervals (C_{inter}). The low-frequency oscillation in CHAR (C_{back}) was interpreted through a locally weighted regression encompassing a 1000-year duration. The high-frequency CHAR (C_{peak}) was derived by subtracting C_{back} from C_{inter}. Notably, C_{peak} is an amalgamation of C_{noise} (perturbations arising from sediment amalgamation, sampling procedures, and analytical processes) and C_{fire} (actualized fire occurrences within a 1 km radius). The distribution of C_{noise} was discerned using a Gaussian mixture model, and a 95% demarcation was employed to categorize samples into distinct "fire" and "non-fire" classifications. To deduce local fire occurrences, the fire frequencies were subjected to a smoothing process over a 1000-year window, expressed as fires per 1000 years.

To explore the interaction of wildfire, climate, and vegetation, the pollen richness index (PRI), and the pollen diversity index (PDI) were estimated using the previously published pollen data from the same region (Liew et al., 2006). Palynological richness can be assessed through rarefaction analyses (Birks and Line, 1992). It is crucial to understand that the purpose of rarefaction is to standardize comparisons by estimating the number of species in samples of equal size. However, this method is limited to making predictions within the range of the observed data. It cannot predict the species count for sample sizes larger than those already collected. The pollen dataset from the previous palynological study consists of 115 samples containing 89 pollen taxa and with sample counts of 1522–390 grains. Thus, PRI was calculated based on a rarefaction analysis of a pollen count of 390 grains. Matthias et al. (2015) sampled the surface sediments of 50 lakes in NE Germany and compared modern pollen deposition with vegetation abundance and landscape patterns. They found that local vegetation diversity is closely correlated to rarefaction to the number of pollen taxa in a theoretical count of 10. Thus, PDI was calculated based on a rarefaction analysis of a pollen count of 10 grains. For the correlation analysis, we resampled our high-resolution records to fit the previous pollen records. The diversity estimates of the previous pollen data, resampling data of this study, and

Table 1
Lab codes, depth, ^{14}C ages, and associated errors of the peat samples.

Lab Code	Depth (cm)	^{14}C Age (kyr BP)	error (ka BP, ± 2σ)	Calibrated ages (kyr BP)	error (ka BP, ± 2σ)
NTUAMS-6106-1	40	2.08	0.07	2.03	0.14
NTUAMS-6107	60	2.35	0.07	2.42	0.12
NTUAMS-6108	90	3.26	0.07	3.5	0.14
NTUAMS-6109-1	120	4.1	0.07	4.67	0.16
NTUAMS-6110-1	150	4.9	0.07	5.67	0.09
NTUAMS-6111-1	168	4.91	0.07	5.67	0.09
NTUAMS-6089-1	168	5.23	0.08	6.05	0.17
NTUAMS-6090	173	5.17	0.08	5.94	0.2
NTUAMS-6091-1	208	5.56	0.09	6.37	0.19
NTUAMS-6092-1	253	5.71	0.09	6.49	0.19
NTUAMS-6093	268	6.14	0.08	7.05	0.21
NTUAMS-6094-1	308	7.04	0.08	7.84	0.15
NTUAMS-6095-1	358	7.32	0.08	8.15	0.17
NTUAMS-6096-1	399	7.91	0.09	8.76	0.22
NTUAMS-6097-1	458	8.75	0.1	9.76	0.21
NTUAMS-6098-1	503	9.29	0.11	10.49	0.27
NTUAMS-6099-1	558	9.64	0.12	10.96	0.29
NTUAMS-6100 b	608	10.51	0.1	12.39	0.28
NTUAMS-6101-1	658	12.17	0.1	14.04	0.28
NTUAMS-6102-1	708	13.25	0.09	15.93	0.25
NTUAMS-6103-1	758	14.28	0.21	17.36	0.54

correlation analysis were carried out in R using the "vegan", "prospectr", "Hmisc", and "corrplot" packages (Wei et al., 2021; McGlinn et al., 2021; Oksanen et al., 2022; Stevens et al., 2022; Harrell and Dupont, 2023).

3. Results

3.1. Elemental concentrations of C–N and carbon isotopic composition

The temporal profile of carbon isotopic composition of total organic carbon ($\delta^{13}C_{TOC}$), total organic carbon (TOC), total nitrogen (TN) contents, and their elemental ratios (TOC/TN) in the Toushe Basin sediment core are shown in Fig. 3. The $\delta^{13}C_{TOC}$ varied greatly from −29.45 to −16.68‰ with an average of −25.33 ± 2.57‰. The $\delta^{13}C_{TOC}$ showed very high values, greater than −20.00‰ between 17.3 and 15.6 cal kyr BP. The average value of $\delta^{13}C_{TOC}$ was −18.67 ± 1.45‰ during that period. The $\delta^{13}C_{TOC}$ values mostly varied from −29.45 to −22.23‰ during 15.6–2.0 cal kyr BP. The $\delta^{13}C_{TOC}$ showed a trend of higher values from 17.3 to 14.5 cal kyr BP, followed by a decrease during 14.5–12.8 cal kyr BP. Between 12.8 and 2.0 cal kyr BP, peaks of higher $\delta^{13}C_{TOC}$ were noticed during 12.8–11.8, 11.0–9.0, 8.5–7.0, 6.5–4.0, and 2.8–2.0 cal kyr BP, while peaks of lower $\delta^{13}C_{TOC}$ were observed during 11.8–11.0, 9.0–8.5, 7.0–6.5, and 4.0–2.8 cal kyr BP.

The TOC and TN contents in the Toushe Basin peatland samples varied from 2.64 to 57.92% and 0.17 to 2.32%, respectively (Fig. 3). The

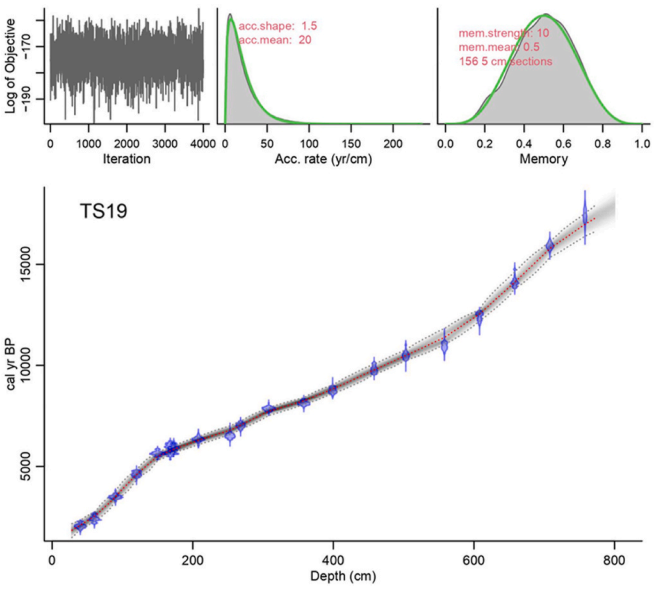

Fig. 2. Bayesian age-depth model of peat deposits from the Toushe Basin (TS19) constructed using the R package 'rbacon' (Blaauw et al., 2021). The blue bars indicate the calibrated ^{14}C ages. Grey dots indicate the model's 95% probability intervals. The dotted red line follows the mean ages. The top left panel shows the Markov Chain Monte Carlo iterations. The middle and right panels show the prior (lines) and posterior densities (area fills) for the mean accumulation rate and memory, respectively.

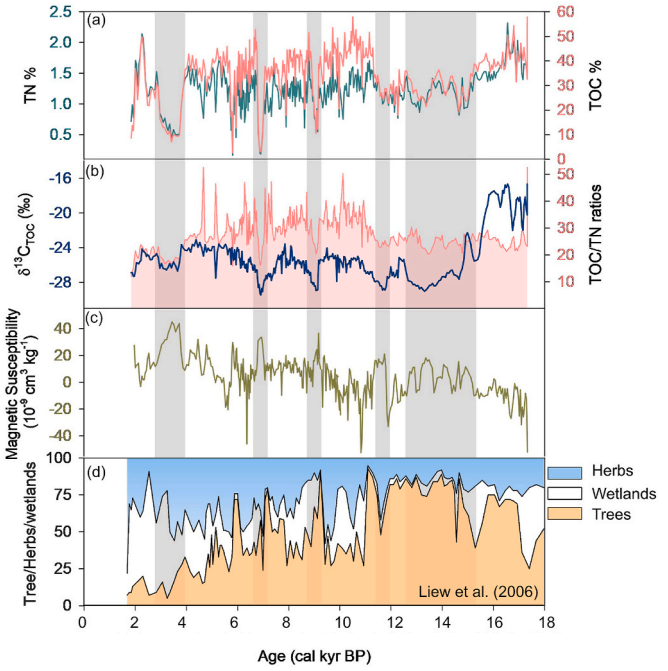

Fig. 3. (a) TOC and TN contents, (b) $\delta^{13}C_{TOC}$ and TOC/TN ratios (b) TOC content, (c) Magnetic susceptibility (MS), and (d) Tree, herb, and wetlands population in the Toushe Basin (Liew et al., 2006). The grey shade bars represent wetter climate conditions in the region.

average TOC and TN contents were 34.57 ± 10.12% and 1.23 ± 0.32%, respectively. The TOC and TN content profiles followed the trend of $\delta^{13}C_{TOC}$ (Fig. 3). All phases with high $\delta^{13}C_{TOC}$ showed high TOC and TN contents, and phases with low $\delta^{13}C_{TOC}$ showed low TOC and TN contents. The TOC and TN showed a decreasing trends during 17.3–12.8 cal kyr BP. Peaks of higher TOC and TN were observed during 12.8–11.8,

11.0–9.0, 8.5–7.0, 6.5–4.0, and 2.8–2.0 cal kyr BP and lower peaks were noticed 11.8–11.0, 9.0–8.5, 7.0–6.5, and 4.0–2.8 cal kyr BP.

Unlike TOC and TN contents, the profile of TOC/TN produced an irregular pattern and did not follow the $\delta^{13}C_{TOC}$ trend (Fig. 3). The TOC/TN ratio of samples varied from 11.76 to 52.54, with an average of 28.18 ± 6.09. The TOC/TN ratios follow the patterns of TOC and TN, showing higher values at 12.8–11.8, 11.0–9.0, 8.5–7.0, 6.5–4.0, and 2.8–2.0 cal kyr BP, and lower values at 11.8–11.0, 9.0–8.5, 7.0–6.5, and 4.0–2.8 cal kyr BP, except for the period from 17.3 to 12.8 cal kyr BP, which shows lower values.

3.2. Magnetic susceptibility

In the current study, the magnetic susceptibility (MS) of Toushe Basin sediments exhibited large fluctuations, representing changes in terrigenous influx into the Toushe Basin during 17.3–2.0 cal kyr BP (Fig. 3c). The MS showed an increasing trend from 17.3 to 12.8 cal kyr BP, followed by a gentle decline during 12.8 to 11.8 cal kyr BP. Subsequently, there was a sudden rise in MS during 11.8 to 11.0 cal kyr BP. Similarly, higher MS values were observed during 9.0–8.5, 7.0–6.5, and 4.0–2.8 cal kyr BP. Low MS values occurred intermittently during 11.0–9.0, 8.5–7.0, 6.5–4.0, and 2.8–2.0 cal kyr BP.

3.3. CHAR and fire frequency

CHAR was estimated to reconstruct the wildfire history and fire frequency per 1000 years in the Toushe Basin (Figs. 4 and 5). The CHAR record showed higher values during 17.3–14.5 cal kyr BP. The fire frequency ranged between 1 and 3 during the same time period. CHAR showed relatively low values during 14.5–11.5 cal kyr BP, with a slight increasing trend towards 11.5 cal kyr BP. The fire frequency varied between 1 and 2 during this period. Low values of CHAR were noticed during 11.5–7.0 cal kyr BP, along with a fire frequency of 2–4 peaks per 1000 years. Subsequently, an increasing trend of CHAR was observed during 7.0–5.0 cal kyr BP. The fire frequencies were lower during this time frame, varying between 0 and 3. The increasing trend of CHAR continued towards 2.0 cal kyr BP. The fire frequencies during this period were much higher, with variation from 1 to 5.

4. Discussion

4.1. Climate reconstruction

A previous study by Huang et al. (2020) reported that the Toushe peatland basin underwent periods of elevated water levels, transitioning into an open-water lacustrine environment, indicating oscillations in water levels in its distant past. These changes in water level governed

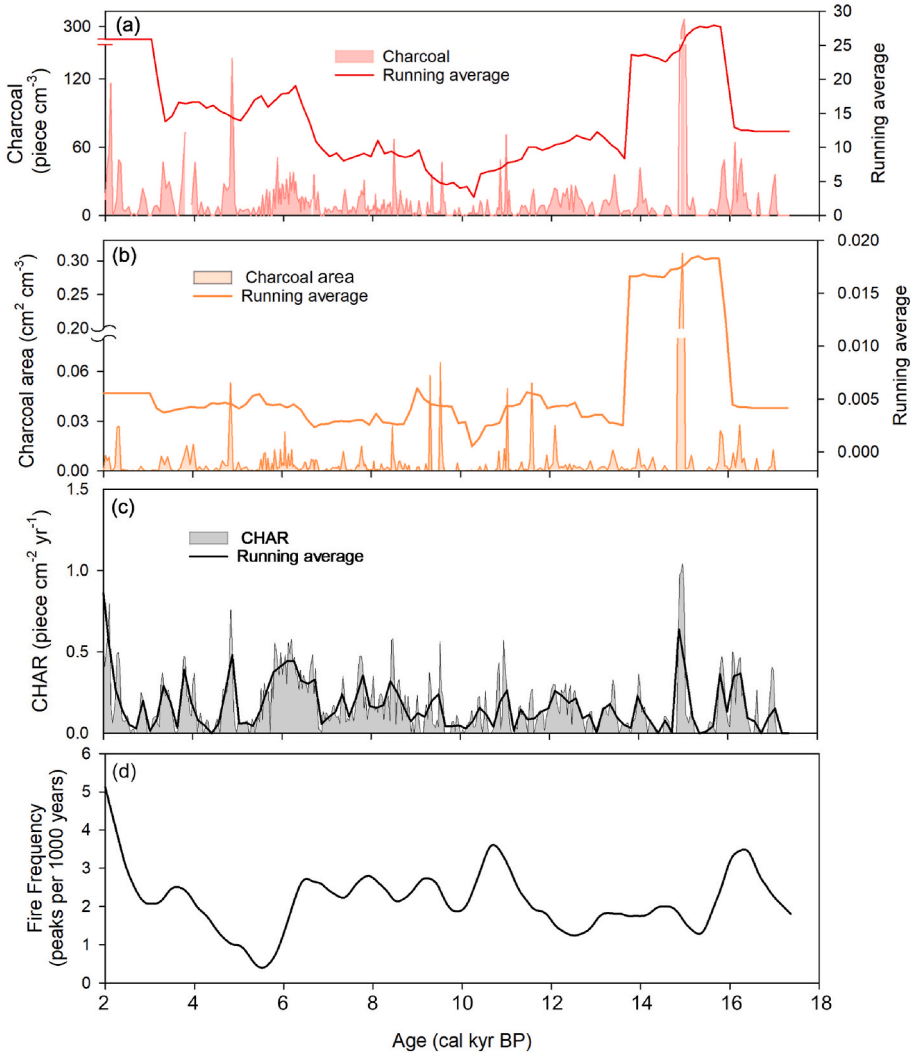

Fig. 4. Temporal profiles of (a) charcoal (piece cm^{-3}), (b) charcoal area (cm^2 cm^{-3}), (c) CHAR (piece cm^{-2} yr^{-1}), and (d) fire frequency (peaks per 1000 years) from the sediment core of the Toushe Basin. The solid line in figure a, b, and c are the running averages (sample proportion = 0.01).

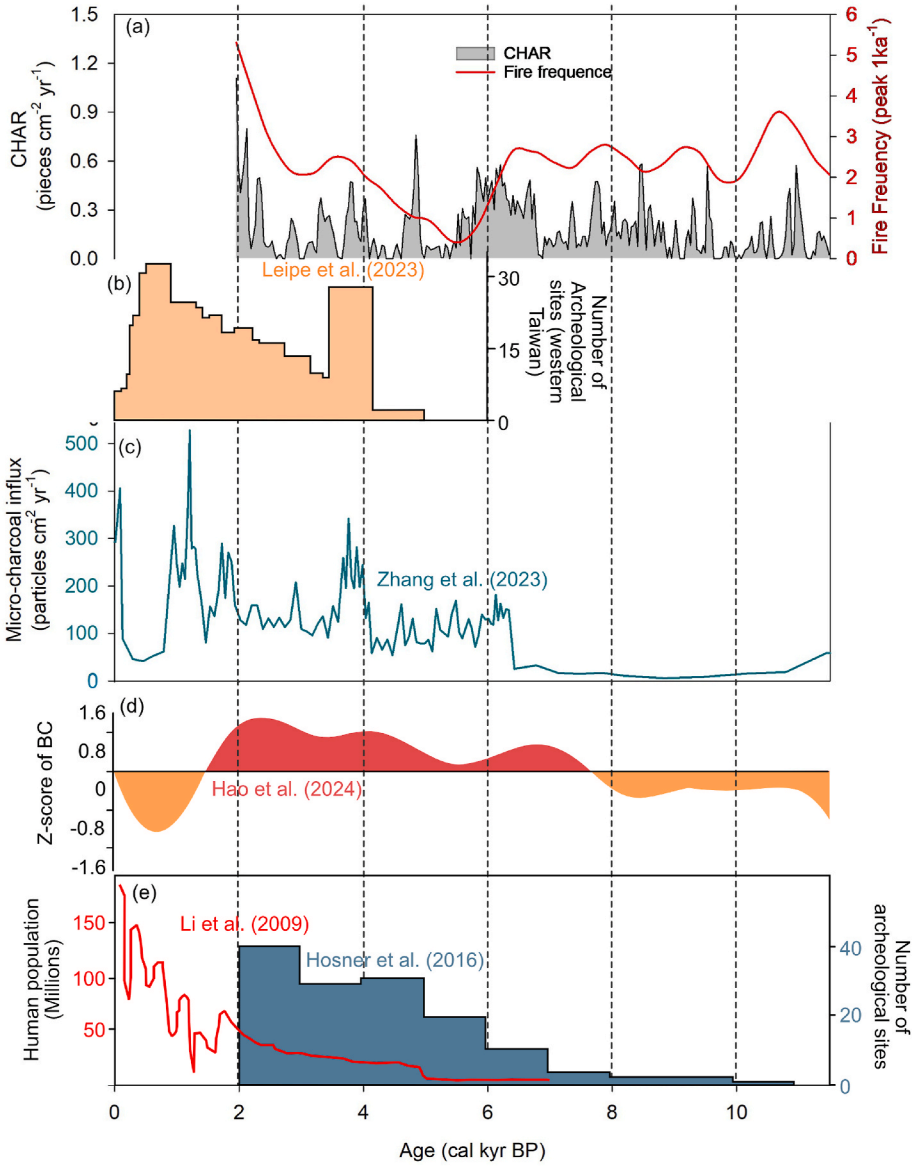

Fig. 5. (a) Fire frequency and CHAR records of Toushe Basin, (b) number of archeological sites in the western Taiwan (Leipe et al., 2023), (c) micro-charcoal flux in Qinling Mountains of east-Central China (Zhang et al., 2023), (d) Z-scores of the BC (black carbon) from Changjiang (Yangtze River) Basin, northern China (Hao et al., 2024), and (e) the population change (red line) (Li et al., 2009) and number of archeological sites (blue bars) in China (Hosner et al., 2016).

the dynamics of vegetation in the peatland region (Laiho et al., 2003; Kokkonen et al., 2019; Zhong et al., 2020). Under high water levels and waterlogged conditions, wetland plants, such as Cyperaceae, flourished (Wang and Kemball, 2005; Liu et al., 2020). Conversely, during low water levels, when the surface is exposed to the atmosphere, herbaceous plants and large trees dominate the region (Pezeshki, 2001; Touchette et al., 2008). These different plants type have distinct $\delta^{13}C$ signature, for example, Cyperaceae and tree are generally C3 plants and exhibited $\delta^{13}C$ values ranges between −32 and −20 ‰, on the other hand, herbaceous plants are largely C4 plants, having $\delta^{13}C$ values range from −16 to −9 ‰ (Carmo-Silva et al., 2008; Wu, 2009; Kohn, 2010; Ellsworth and Cousins, 2016). A previous study also showed a positive correlation between $\delta^{13}C$ of Toushe Basin organic matter and change in vegetation dynamics; suggested $\delta^{13}C$ of Toushe Basin organic matter is a robust indicator of inferring about past vegetation (C3 and C4) changes (Meyers, 2003; Li et al., 2013). This point towards the change in climatic conditions; the C3 plants are an indicator of wetter climate and C4 plants are for the drier climate (Meyers, 2003; Liew et al., 2014; Rahman et al., 2020; Shah et al., 2022, 2023). In addition, TOC/TN ratios provide information about changes in climate conditions by inferring changes in the source of organic matter (Meyers, 1997, 2003). In general, in-situ production exhibits low TOC/TN ratios (<10), while land plants have high TOC/TN ratios (>20) (Meyers, 2003). In the current scenario, increasing water levels support wetland species in the region, resulting in lower TOC/TN ratios (Janyszek-Sołtysiak et al., 2021; Larson, 1995; H. Li et al., 2019). On the other hand, during low water levels caused by drier climate, herbaceous plants and trees will dominate the basin, resulting in higher TOC/TN ratios (Cheng et al., 2006; Hudon et al., 2005).

Between 17.3 and 12.8 cal kyr BP, a decreasing trend in $\delta^{13}C_{TOC}$, TOC, and TN were observed, along with consistently low TOC/TN ratios (Fig. 3). The decreasing trend of $\delta^{13}C_{TOC}$ suggested an increase in dominance of C3 plants from 17.3 to 12.8 cal kyr BP, indicating transitioning of climate from drier to wetter. During the same timeframe, the previous records indicated lower wetlands, a moderate decrease in herbaceous plants, and an increase in tree species, supporting the current interpretation. The change in climate from dry to wet, can also influence the runoff conditions of the region. The TOC/TN, which is an

indicator of runoff (Meyers, 2003; Rahman et al., 2020), did not show any significant change. However, the MS, an indicator of magnetic minerals inputs (Thompson et al., 1975; Demory et al., 2005), showed a gradual increase during this time interval, suggesting an increase in terrigenous sediments to the Toushe Basin, which indicated an increase in runoff conditions. This increase in runoff also diluted organic matter, represented by the decreasing trends of TOC and TN, in the Toushe Basin during 17.5–12.8 cal kyr BP. The organic matter dilution through higher sedimentary flux has been previously reported from the Dream Lake, Taiwan, and Wular Lake, Kashmir Himalaya, India (Shah et al., 2020; Rahman et al., 2024).

The $\delta^{13}C_{TOC}$ showed slightly higher values between 12.8 and 11.8 cal kyr BP, suggesting an increase in C4 vegetation cover, which is also supported by a high population of herbaceous plants in the region (Fig. 3). In addition, trees also showed slightly higher values, while the wetlands were lower. This indicates a decrease in runoff and a dominance of terrestrial plants in the region, which is reflected in higher TOC/TN ratios between 12.8 and 11.8 cal kyr BP (Fig. 4). Concurrently, lower MS indicated reduced runoff conditions, leading to a lower water table and the flourishing of herbaceous C4 plants in the region, signaling drier climate conditions. The observed peaks in TOC and TN contents suggest increased organic matter deposition during this period, likely due to reduced sediment dilution of organic matter. The previous pollen and isotope studies from the Toushe Basin have also indicated drier climate condition during this interval, aligning with the globally recognized Younger Dryas event (Li et al., 2013; Liew et al., 2006). Similar situations were noticed during 11.0–9.0 cal kyr BP, 8.5–7.0, 6.5–4.0, and 2.8–2.0 cal kyr BP which indicated drier climate conditions.

Low $\delta^{13}C_{TOC}$, TOC, TN, and TOC/TN were observed, along with high MS during 11.8–11.0, 9.0–8.5, 7.0–6.5, and 4.0–2.8 cal kyr BP. Interestingly, during these time intervals, pollen data showed high wetland plants, indicating a rise in the water table. A previous study showed Cyperaceae were one of the dominant wetland plants in the study region and generally exhibited TOC/TN ratios within a narrow range of 10.3–16.3 (Janyszek-Sołtysiak et al., 2021). Although the sedge family (Cyperaceae) can contain both C3 and C4 plants, Wu (2009) investigated the species of Cyperaceae in Taiwan and found that C4 plants accounted for only 35%. Previous studies reported the dominance of C3-type Cyperaceae in mountainous aquatic environments, comparable to our study region (Tieszen et al., 1979; Chmura and Aharon, 1995; Rajagopalan et al., 1999; Malamud-Roam and Ingram, 2004; Larridon et al., 2011). Moreover, a comprehensive review reveals that the $\delta^{13}C$ values of C3 Cyperaceae species are varied from −34 to −25 ‰ (Larridon et al., 2011). Furthermore, the periods of low $\delta^{13}C_{TOC}$ were associated with increased tree coverage in the catchment area. Concurrently, elevated MS levels that indicated enhanced runoff, likely transported C3 plants derived organic matter into the lake. This increased runoff, a result of larger sedimentary fluxes in the basin, also led to the dilution of organic matter, as evidenced by reduced TOC and TN contents. Overall, it appeared that climate conditions were wetter during the time intervals of 11.8–11.0, 9.0–8.5, 7.0–6.5, and 4.0–2.8 cal kyr BP.

4.2. Reconstructed wildfire activity

Macro-charcoal (>125 μm) analysis suggests a pronounced shift in the local fire regime around the Toushe Basin from 17.5 to 2.0 cal kyr BP (Fig. 4). The high CHAR data represents a high-severity fire regime during 17.3–14.5 cal kyr BP and 5.0–2.0 cal kyr BP. Low CHAR indicates a low-severity fire regime during 14.5–5.0 cal kyr BP. Fire severity is defined as the extent of above and below-ground biomass consumed by a fire, which is reflected in the overall quantity of charcoal deposited in the lake. Whereas, the fire intensity serves as a gauge of energy output (Keeley, 2009). Elevated fire intensities typically result in greater fire severity, leading to distinct effects on vegetation and recovery when compared to low-intensity fires (Rogers et al., 2015).

A high abundance of charcoal in lake sediments suggests an increased amount of biomass burned in each fire, more intense fires, more frequent fires, or a combination of all three factors. However, the temporal resolution of the charcoal records is too low to apply common peak detection methods to identify individual fire events, however, magnitude of CHAR peaks suggest the amount of biomass burning (Whitlock and Larsen, 2001). The relative comparison of CHAR peaks during the current study revealed higher values during 17.3–14.5 cal kyr BP and 5.0–2.0 cal kyr BP and lower values during 14.5–5.0 cal kyr BP. This suggests high-severity fires during the 17.3–14.5 cal kyr BP and 5.0–2.0 cal kyr BP and low-severity fires during 14.5–5.0 cal kyr BP. As the severity was also measured through loss of organic matter through wildfire, a negative correlation was noticed between TOC in the sediments and charcoal during the current study (Table S1). It reflected the loss of organic matter from the region due to high severity wildfire.

The high surface area of charcoal, indicating larger particles, in the prominent CHAR peaks suggests a higher fire intensity during the studied period (Duffin et al., 2008; Hennebelle et al., 2020). Typically, high-intensity fires produce large flames capable of scorching trees and producing larger, more robust charcoal particles (Clark, 1988; Vachula and Richter, 2018). Furthermore, high-intensity fires allow for large charcoal particles to be ejected into the atmosphere within stronger plumes, and these particles are subsequently better preserved during deposition (Clark, 1988; Ward and Hardy, 1991). Conversely, during low-intensity fires, the canopy remains mostly undisturbed, and the lower fire intensities generally do not generate strong convection (Glückler et al., 2022). These two factors restrict the height at which plumes eject and the subsequent dispersion of charcoal particles, resulting in lower CHAR levels (Clark, 1988; Vachula and Richter, 2018). In this study, high charcoal areas during 17.3–14.5 cal kyr BP and 5.0–2.0 cal kyr BP suggested high-intensity fires in the region. On the other hand, low charcoal area points towards low-intensity fire during 14.5–5.0 cal kyr BP.

The increasing wildfire trend observed in the present study aligns with the wildfire patterns documented in north-eastern and central China during the Holocene (Hao et al., 2024; Zhang et al., 2023) (Fig. 5). In China, this increasing trend was attributed to human activities, which were documented as increase in number of archeological sites as well as the population (Hosner et al., 2016; Li et al., 2009). However, the increasing trend of wildfires in Taiwan were attributed to the climate till 5.0 cal kyr BP, and then by the human activities (Leipe et al., 2023). As the human began to settle in the western Taiwan around 5.0 cal kyr BP (Fig. 5). The increasing trend of number of archeological sites in western Taiwan suggesting that high intensity fires were dominantly human-induced.

4.3. Wildfire-vegetation-climate-human interaction

The intricate relationships among wildfires, vegetation, climate, and human activity make it difficult to isolate distinct causes purely through statistical analysis in paleoenvironmental research. In this study, we conducted a comparative analysis of peak occurrences in wildfires, climate proxies, and changes in vegetation within the Toushe Basin (Fig. 6). In the Toushe Basin, the combination of two pollen-based studies revealed that during 17.3–2.0 cal kyr BP, temperate deciduous forests and mixed coniferous forests were the prevailing vegetation types (Li et al., 2013). The time frame from 11.5 to 7.0 cal kyr BP marked a transitional phase, shifting from deciduous and mixed coniferous forests to warm-temperate forests. Subsequently, there was a transformation to subtropical evergreen forests during 7.0–2.0 cal kyr BP.

The observed high intensity fire during 17.3 to 14.5 cal kyr BP, appeared to be due to drier climate conditions in the region (Fig. 6). It is believed that the drier climate is one of major cause of high intensity fire globally (Greisman and Gaillard, 2009; Stephens et al., 2018; Zumbrunnen et al., 2009). This time frame of high intensity fire characterized by low population of wetlands in Toushe Basin, suggesting the

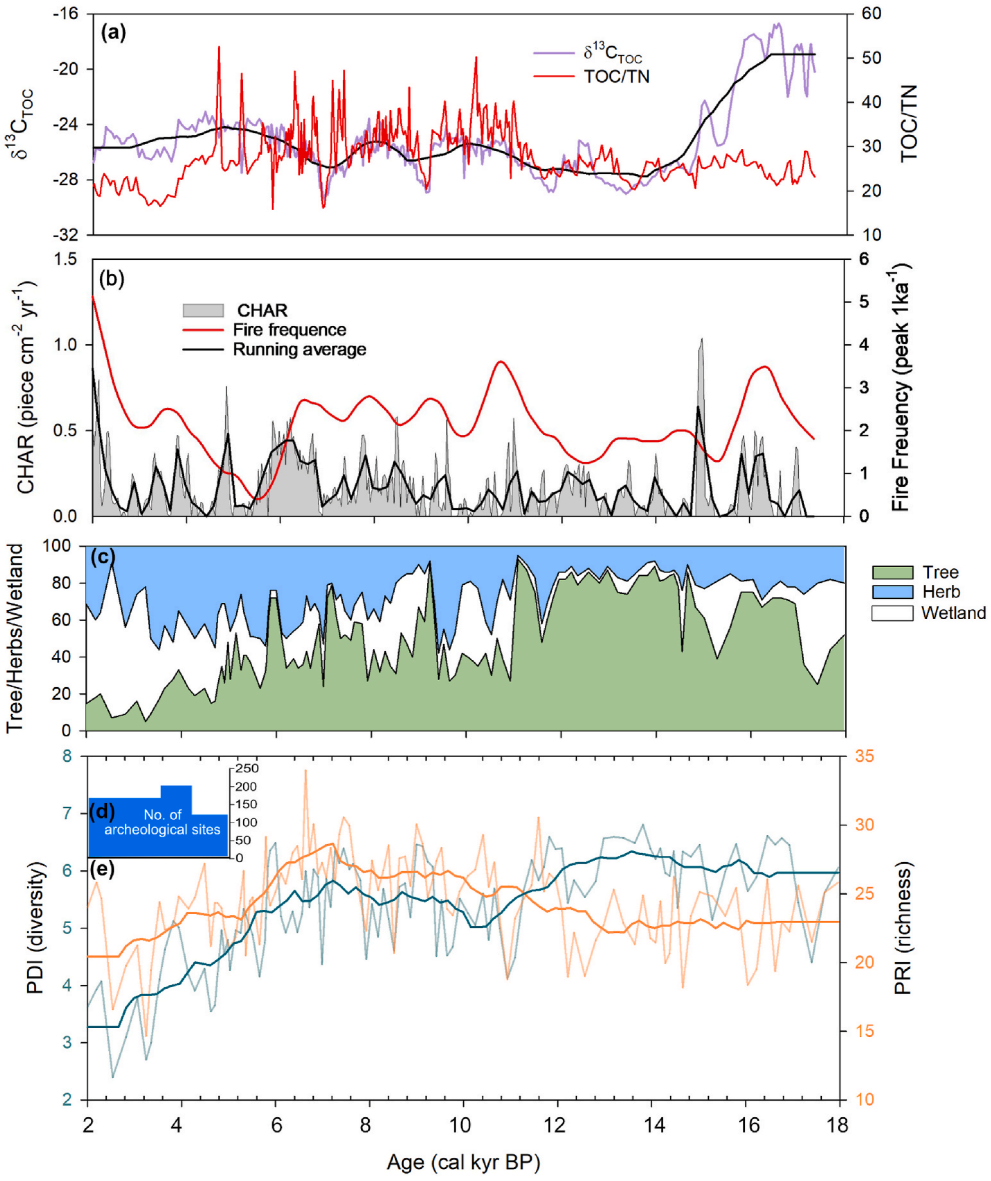

Fig. 6. (a) $\delta^{13}C_{TOC}$ and TOC/TN ratios, (b) fire frequency and CHAR records of Toushe Basin, (c) Tree, herb, and wetland plant percentages in the Toushe Basin during the studied period (Li et al., 2013), (d) number of archeological sites in Taiwan (Leipe et al., 2023), and (e) pollen diversity index (PDI) and pollen richness index (PRI), represent the vegetation diversity, in the Toushe Basin. PDI and PRI were estimated using published pollen data (Liew et al., 2006).

burning of wetland plants. Wetland plants typically inhabit more moist, less fire-prone environments; however, prolonged periods of dry climate can lower the water level in wetlands, leaving organic matter such as peat and plant biomass dry and susceptible to burning (Blake et al., 2021; Zhong et al., 2020). A slight decrease in the populations of trees was observed during periods of high intensity fire, implying that, beyond wetlands, trees also functioned as biofuel sources. The previous studies have shown that stronger winds and a drier climate allowed fires in lower altitude to spread into adjacent forest regions, burning woody vegetation and resulting in high-severity fires (McCutchan and Fox, 1986; Maynard, 2013; Meigs et al., 2020). The modern climate observations clearly suggest high wind speed during the winter season, from November to March, in Taiwan (Kuo and Ho, 2004; Ren et al., 2022). The drier climates and strong wind conditions were responsible for increased vegetation dryness, rendering it more susceptible to high-intensity fires during 17.3–15.8 cal kyr BP. Consequently, the fire in wetland and trees caused a decline of the ecological heterogeneity of the region, as evidenced by the decrease in PDI and PRI.

At 15.0 cal kyr BP, high intensity fires were observed due to a drier climate, corresponding to a decrease in wetlands population – suggesting the burning of wetland plants. Trees and herbs showed relatively high values during this time, indicating that wildfires shaped the landscape's ecosystem, transitioning it from being dominated by wetlands to being dominated by trees and herbaceous plants. This transformation opened up habitats for trees and herbaceous plants to colonize, resulting in an ecological diversification in the Toushe Basin, as shown by high PDI and PRI.

Low-intensity fire and relatively low fire frequencies were observed during 14.5–11.5 cal kyr BP (Fig. 6). Previous records suggested a temperate and less dry climate (Li et al., 2013), and the current $\delta^{13}C_{TOC}$ record indicates a wetter climate during this time interval. In addition, high tree percentages (up to 85%) were noticed during this period, along with the decrease in wetland taxa (Li et al., 2013). Low intensity fires during this period were attributed to the low herbs and wetland plants in the region, along with high trees, indicating the burning of herbaceous and wetland plants in the region, with possibly fires mainly confined to the basin. The high trees, during the time intervals of low intensity fires, indicated that fire likely transformed the basin vegetation from

herbaceous and wetland plants to forests. It has been reported that increased moisture in a wetland region acted as a deterrent to fire spread (Rossa et al., 2016). It has been well-documented in previous studies that the presence of wet peat surface conditions effectively inhibits the spread of fires into the surrounding forests (Page et al., 2009; Feurdean et al., 2022). Furthermore, it is plausible that the wetter conditions during this time period reduced the flammability of trees, as suggested by several studies that have highlighted the pivotal role of plant moisture content in determining their flammability (Kreye et al., 2020; Varner et al., 2015). The widespread growth of various tree species during this period likely enhanced pollen diversity, as indicated by a higher PDI during 14.5–11.5 cal kyr BP. However, this shift likely reduced habitat heterogeneity due to low-intensity fires, affecting the variety of niches available for different species of herbaceous and wetland plants, and leading to overall lower PRI.

Low-intensity fires continued during 11.5–5.0 cal kyr BP, along with high fire frequencies, which appeared to be the cause of relatively drier climate conditions in the region, represented by high $\delta^{13}C_{TOC}$ (Fig. 6). In addition, the majority of the low CHAR peaks coincided with diminished wetlands, suggesting the burning of wetlands in the region. The tree population also appeared to be smaller during periods of low-intensity fires, indicating that the strong winds during these drier intervals were moving toward the adjacent forests. Conversely, herbs exhibited either an increasing trend or maintained high values during periods of low-intensity fires burning between 11.5 and 5.0 cal kyr BP. This suggested that low-intensity fires in the Toushe Basin were facilitating the opening of the area, resulting in the predominance of herbaceous plants. Fire increases in soil nutrient availability have been reported widely (Anderson and Menges, 1997; Fuentes-Ramirez et al., 2015), which likely enhanced the growth of herbaceous plants and transformed the ecological landscape of the Toushe Basin towards a grassland. In addition, the decreasing trend of CHAR indicated a reduction in fire intensity approaching 10.0 cal kyr BP, followed by an increase towards 6.0 cal kyr BP. This trend covaried with the pattern of PDI. On the other hand, PRI also covaried from 10.0 to 6.0 cal kyr BP with an increasing trend. This indicated that an increase in fire intensity during this time period controlled ecosystem diversity by increasing the abundance and different species of herbaceous plants.

During 5.0–2.0 cal kyr BP, the escalation of high-intensity fires and a notable increase in fire frequencies were noticed and appeared to be linked with expanding human presence in the region (Figs. 5 and 6). A recent study showed that humans began to settle down in Taiwan from 5.0 kyr BP (Leipe et al., 2023). They showed an increasing trend in the number of sites per 100 years in western Taiwan during the last 5.0 cal kyr BP. It pointed towards the change in the ignition source from natural to anthropogenic. During this period, the overall climate conditions were wetter. In general, the wetter climate enhances the tree moisture condition, which possibly reduced tree flammability. However, in the current study, during 5.0–2.0 cal kyr BP, a gradual decline in the populations of trees and herbaceous plants was noticed, alongside an expansion of wetlands. This decrease in tree population pointed towards the possibility of land clearing using slash-and-burn methodology, and the wetter climate conditions at this time led to waterlogged conditions and a subsequent expansion of wetland areas. It suggested that human-induced burning likely contributed as an additional factor to the high intensity of fires during 5.0–2.0 cal kyr BP. Documentation of increased human activity in western Taiwan by Leipe et al. (2023) supports our hypothesis of human presence in the region during 5.0–2.0 cal kyr BP. In contrast, Huang et al. (2020) indicated that the region began to be affected by human activities after 2.1 cal kyr BP, based on the presence of Poaceae (>37 μm) and *Typha*. The absence of direct evidence makes our interpretations uncertain, suggesting that additional studies, like archeological sites or analysis of fecal biomarkers (which indicate past human and animal activity), are needed to confirm our hypothesis.

4.4. Possible causes of wildfires in central Taiwan and their connection to El- Niño activity

Climate and wildfire collectively affected vegetation diversity in the Toushe Basin over the long term. Additionally, it has been observed that peaks of CHAR coincided with peaks in El-Niño like conditions, which are characterized by low sea surface temperature differences between the western Pacific warm pool and the eastern equatorial pool (WPWP-EEP (ΔSST)) (Wara et al., 2005; Jia et al., 2018) (Fig. 7). El-Niño events are associated with decreased rainfall in Taiwan, likely due to a weakened East Asian Summer Monsoon EASM (Li et al., 2013; Wang et al., 2015). A study has shown that Eastern Asia experiences a very high flash rate of lightning during El-Niño events (Yoshida et al., 2007). Lightning, along with biomass fuel, temperature, oxygen, and moisture, plays an important role in severe wildfire activities worldwide (Johnson et al., 2011; Krause et al., 2014; Yedinak et al., 2018). In the Taiwan region, biomass and oxygen are sufficiently available, while temperature and moisture vary with changes in Pacific Ocean sea surface temperatures (Hsu et al., 2001). During El-Niño events, when humidity decreases, the ignition temperature decreases, making it easier for wildfires to start and spread (Chen et al., 2004; Demirbas, 2004; Vamvuka and Sfakiotakis, 2011; Littell et al., 2016). A previous study has also found a similar relationship between wildfires and El-Niño like conditions in the Toushe Basin during the mid to late Holocene (Huang et al., 2020). Therefore, it appears that long periods of drought and El-Niño like conditions caused extreme dryness in the region, leading to high-intensity fires. On the other hand, long periods of wetter climate, characterized by shorter intervals of weaker El-Niño like conditions, likely caused the low-severity wildfires in the region.

5. Conclusion

The current study has highlighted the wildfire, vegetation, climate, and human interaction in the central Taiwan region from 17.3 to 2.0 cal kyr BP.

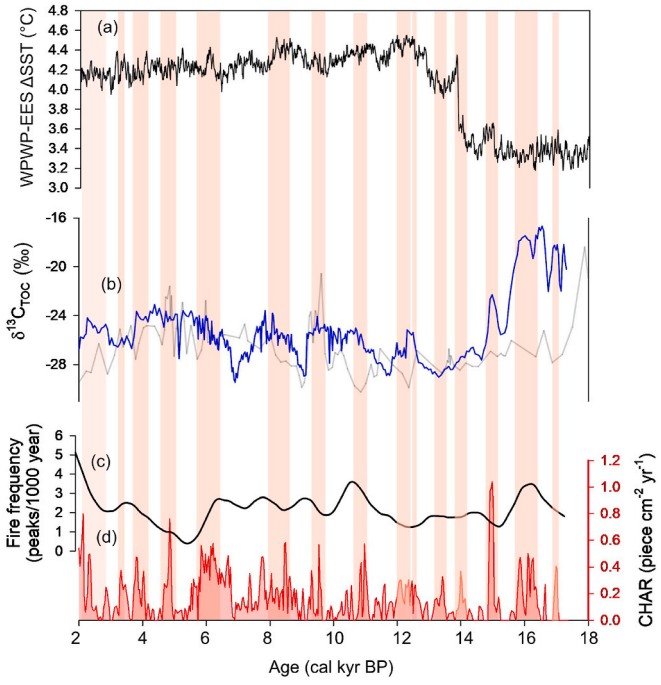

Fig. 7. Comparison of the wildfire records with regional climate and change in sea temperature of Pacific Ocean. (a) WPWP-EEP (ΔSST), (b) $\delta^{13}C_{TOC}$ of the current study (blue line) and Li et al. (2013) (grey line), (c) fire frequency, and (d) CHAR records of Toushe Basin. The orange color shaded bars showed time frame of coincidence of high CHAR, high $\delta^{13}C_{TOC}$, and low WPWP-EEP (ΔSST).

- The current study showed an improvement in climate conditions from 17.3 to 12.8 cal kyr BP, followed by a drier period between 12.8 and 1L.8, coinciding with the Younger Dryas. Furthermore, the drier climate conditions were recorded during 11.0–9.0 cal kyr BP, 8.5–7.0 cal kyr BP, 6.5–4.0 and 2.8–2.0 cal kyr BP with intermittent wetter climate conditions during 11.8–11.0 cal kyr BP, 9.0–8.5 cal kyr BP, 7.0–6.5 cal kyr BP, and 4.0–2.8 cal kyr BP.
- The drier climate largely controlled the wildfires in the central Taiwan region. The current study showed high-intensity fires were observed during the 17.3–14.5 cal kyr BP, caused by a drier climate, and during 5.0–2.0 cal kyr BP was due to human-induced burning. The low intensity fire noticed from 14.5 to 5.0 cal kyr BP, due to relatively humid conditions in the region.
- In the Toushe Basin, from 17.5 to 5.0 cal kyr BP, frequent wildfires predominantly affected wetlands and forested areas, facilitating a shift in vegetation dynamics towards the dominance of herbaceous species. Conversely, during the interval from 5.0 to 2.0 cal kyr BP, the region experienced a marked shift in fire regimes, with an increased incidence of fires affecting both arboreal and herbaceous vegetation. The observed changes in the Toushe Basin's vegetation were predominantly driven by wildfire dynamics, underscoring the profound impact of fire regimes on ecological transformations within the region.
- Additionally, it has been also noticed the wildfires in the Toushe basin were the result of the El-Niño event that induced longer or shorter drier climate conditions in the region.

The current study has discussed about the likelihood of humans-induced wildfires between 5.0 and 2.0 cal kyr BP. This speculation is based on the relationship observed amongst climate, vegetation, and fire during the studied period. To further explore this possibility, a thorough investigation of the area is required. This includes looking into archeological evidence and analyzing fecal biomarkers to provide more concrete answers regarding human involvement in past wildfires.

Author contributions

Abdur Rahman: Formal analysis; Investigation; Visualization; Writing – original draft; Writing – review & editing. Yuan-Pin Chang: Methodology; Writing – review & editing. Hong-Chun Li: Methodology; Writing – review & editing. Ling-Ho Chung: Investigation; Methodology. Liang-Chi Wang: Conceptualization; Data curation; Funding acquisition; Investigation; Methodology; Project administration; Resources; Supervision; Validation; Writing – review & editing.

Funding

This research was funded by the National Science and Technology Council, Taiwan (grant number NSTC 112-2116-M-194-018-, 112-2811-M-194-002-, 112-2811-M-194 -001-, 111-2116-M-194-024-, 110-2116-M-194-008-, 109-2116-M-002-022-).

Declaration of competing interest

The authors declare that they have no known competing financial interests or personal relationships that could have appeared to influence the work reported in this paper.

Data availability

Data will be made available on request.

Acknowledgements

We thank Mr. Shun-Yu Wang for allowing us to collect samples on his land and for the help in the filed excursion.

Appendix A. Supplementary data

Supplementary data to this article can be found online at https://doi.org/10.1016/j.quascirev.2024.108820.

References

Acácio, V., Holmgren, M., Rego, F., Moreira, F., Mohren, G.M.J., 2009. Are drought and wildfires turning Mediterranean cork oak forests into persistent shrublands? Agrofor. Syst. 76 (2), 389–400. https://doi.org/10.1007/s10457-008-9165-y.

Anderson, R.C., Menges, E.S., 1997. Effects of fire on sandhill herbs: Nutrients, mycorrhizae, and biomass allocation. Am. J. Bot. 84 (7), 938–948. https://doi.org/10.2307/2446284.

Archibald, S., 2016. Managing the human component of fire regimes: Lessons from Africa. Phil. Trans. Biol. Sci. 371 (1696), 20150346.

Barbero, R., Abatzoglou, J.T., Larkin, N.K., Kolden, C.A., Stocks, B., 2015. Climate change presents increased potential for very large fires in the contiguous United States. Int. J. Wildland Fire 24 (7), 892–899.

Birks, H.J.B., Line, J.M., 1992. The use of rarefaction analysis for estimating palynological richness from quaternary pollen-analytical data. Holocene 2 (1), 1–10. https://doi.org/10.1177/095968369200200101.

Blaauw, M., Christen, J.A., Lopez, M.A.A., Vazquez, J.E., Belding, T., Theiler, J., Gough, B., Karney, C., Rcpp, L., Blaauw, M.M., 2021. Package 'rbacon.

Blake, D., Boyce, M.C., Stock, W.D., Horwitz, P., 2021. Fire in organic-rich wetland sediments: inorganic responses in porewater. Water, Air, Soil Pollut. 232 (3), 101. https://doi.org/10.1007/s11270-021-05013-6.

Carmo-Silva, A.E., Powers, S.J., Keys, A.J., Arrabaça, M.C., Parry, M.A., 2008. Photorespiration in C4 grasses remains slow under drought conditions. Plant Cell Environ. 31 (7), 925–940.

Certini, G., 2005. Effects of fire on properties of forest soils: a review. Oecologia 143, 1–10.

Chen, T., Wang, S., Huang, W., Yen, M., 2004. Variation of the East Asian summer monsoon rainfall. J. Clim. 17 (4), 744–762. https://doi.org/10.1175/1520-0442(2004)017<0744:VOTEAS>2.0.CO;2.

Chen, W.F., Wang, S.Y., Tsai, M.P., 2009. Investigation of improving policy on mountain area flood problem- Toushe Alive Basin in Yuchih township as an example. J. Soil Water Conserv. 41, 467–483.

Cheng, X., Luo, Y., Chen, J., Lin, G., Chen, J., Li, B., 2006. Short-term C4 plant *Spartina alterniflora* invasions change the soil carbon in C3 plant-dominated tidal wetlands on a growing estuarine Island. Soil Biol. Biochem. 38 (12), 3380–3386.

Chmura, G.L., Aharon, P., 1995. Stable carbon isotope signatures of sedimentary carbon in coastal wetlands as indicators of salinity regime. J. Coast Res. 124–135.

Clark, J.S., 1988. Particle motion and the theory of charcoal analysis: source area, transport, deposition, and sampling. Quat. Res. 30 (1), 67–80.

Cochrane, M.A., Bowman, D.M., 2021. Manage fire regimes, not fires. Nat. Geosci. 14 (7), 455–457.

Corona-Núñez, R.O., Li, F., Campo, J.E., 2020. Fires represent an important source of carbon emissions in Mexico. Global Biogeochem. Cycles 34 (12), e2020GB006815.

Dale, V.H., Joyce, L.A., McNulty, S., Neilson, R.P., Ayres, M.P., Flannigan, M.D., Hanson, P.J., Irland, L.C., Lugo, A.E., Peterson, C.J., 2001. Climate change and forest disturbances: climate change can affect forests by altering the frequency, intensity, duration, and timing of fire, drought, introduced species, insect and pathogen outbreaks, hurricanes, windstorms, ice storms, or landslides. Bioscience 51 (9), 723–734.

Demirbas, A., 2004. Combustion characteristics of different biomass fuels. Prog. Energy Combust. Sci. 30 (2), 219–230.

Demory, F., Oberhänsli, H., Nowaczyk, N.R., Gottschalk, M., Wirth, R., Naumann, R., 2005. Detrital input and early diagenesis in sediments from Lake Baikal revealed by rock magnetism. Global Planet. Change 46 (1–4), 145–166.

Duffin, K., Gillson, L., Willis, K., 2008. Testing the sensitivity of charcoal as an indicator of fire events in savanna environments: quantitative predictions of fire proximity, area and intensity. Holocene 18 (2), 279–291.

Ellsworth, P.Z., Cousins, A.B., 2016. Carbon isotopes and water use efficiency in C4 plants. Curr. Opin. Plant Biol. 31, 155–161.

Feurdean, A., Diaconu, A.-C., Pfeiffer, M., Gałka, M., Hutchinson, S.M., Butiseaca, G., Gorina, N., Tonkov, S., Niamir, A., Tantau, I., 2022. Holocene wildfire regimes in western Siberia: interaction between peatland moisture conditions and the composition of plant functional types. Clim. Past 18 (6), 1255–1274.

Flannigan, M., Cantin, A.S., De Groot, W.J., Wotton, M., Newbery, A., Gowman, L.M., 2013. Global wildland fire season severity in the 21st century. For. Ecol. Manag. 294, 54–61.

Foster, C., Barton, P., Robinson, N., MacGregor, C., Lindenmayer, D.B., 2017. Effects of a large wildfire on vegetation structure in a variable fire mosaic. Ecol. Appl. 27 (8), 2369–2381.

Fuentes-Ramirez, A., Schafer, J.L., Mudrak, E.L., Schat, M., Parag, H.A., Holzapfel, C., Moloney, K.A., 2015. Spatio-temporal impacts of fire on soil nutrient availability in *Larrea tridentata* shrublands of the Mojave Desert, USA. Geoderma 259, 126–133.

Ganteaume, A., Syphard, A.D., 2018. Ignition sources. In: Encyclopedia of Wildfires and Wildland-Urban Interface (WUI) Fires, pp. 1–17.

Glückler, R., Geng, R., Grimm, L., Baisheva, I., Herzschuh, U., Stoof-Leichsenring, K.R., Kruse, S., Andreev, A., Pestryakova, L., Dietze, E., 2022. Holocene wildfire and vegetation dynamics in Central Yakutia, Siberia, reconstructed from lake-sediment proxies. Frontiers in Ecology and Evolution 10, 962906.

Greisman, A., Gaillard, M., 2009. The role of climate variability and fire in early and mid Holocene forest dynamics of southern Sweden. J. Quat. Sci. 24 (6), 593–611. https://doi.org/10.1002/jqs.1241.
Guijarro, J.A., 2019. Climatol: climate Tools (series homogenization and derived products). R Package Version 3 (2).
Halofsky, J.E., Peterson, D.L., Harvey, B.J., 2020. Changing wildfire, changing forests: the effects of climate change on fire regimes and vegetation in the Pacific Northwest, USA. Fire Ecology 16 (1), 1–26.
Hao, Q., Tang, M., Huang, X., Zhang, C., Dang, S., Yang, S., 2024. Holocene wildfire regime shifts induced by the enhancement of human activities in the Changjiang (Yangtze River) Basin. Catena 240, 107998.
Harrell, F.E.J., Dupont, C., 2023. *Hmisc: Harrell Miscellaneous* (5.1-1) [R-Packages]. https://cran.r-project.org/web/packages/Hmisc/index.html.
Harrison, M., Meindl, C.F., 2001. A statistical relationship between El-Niño -Southern Oscillation and Florida wildfire occurrence. Phys. Geogr. 22 (3), 187–203.
Hayes, J.P., 2021. Fire suppression and the wildfire paradox in contemporary China: policies, resilience, and effects in Chinese fire regimes. Hum. Ecol. 49 (1), 19–32.
Hennebelle, A., Aleman, J.C., Ali, A.A., Bergeron, Y., Carcaillet, C., Grondin, P., Landry, J., Blarquez, O., 2020. The reconstruction of burned area and fire severity using charcoal from boreal lake sediments. Holocene 30 (10), 1400–1409.
Higuera, P.E., Brubaker, L.B., Anderson, P.M., Hu, F.S., Brown, T.A., 2009. Vegetation mediated the impacts of postglacial climate change on fire regimes in the south-central Brooks Range, Alaska. Ecol. Monogr. 79 (2), 201–219. https://doi.org/10.1890/07-2019.1.
Hosner, D., Wagner, M., Tarasov, P.E., Chen, X., Leipe, C., 2016. Spatiotemporal distribution patterns of archaeological sites in China during the Neolithic and Bronze Age: an overview. Holocene 26 (10), 1576–1593.
Hsu, H.-H., Chen, Y.-L., Kau, W.-S., 2001. Effects of atmosphere-ocean interaction on the interannual variability of winter temperature in Taiwan and East Asia. Clim. Dynam. 17, 305–316.
Huang, Z., Ma, C., Chyi, S.-J., Tang, L., Zhao, L., 2020. Paleofire, vegetation, and climate reconstructions of the middle to late Holocene from lacustrine sediments of the Toushe Basin, Taiwan. Geophys. Res. Lett. 47 (20), e2020GL090401 https://doi.org/10.1029/2020GL090401.
Hudon, C., Gagnon, P., Amyot, J.-P., Létourneau, G., Jean, M., Plante, C., Rioux, D., Deschênes, M., 2005. Historical changes in herbaceous wetland distribution induced by hydrological conditions in Lake Saint-Pierre (St. Lawrence River, Quebec, Canada). Hydrobiologia 539 (1), 205–224. https://doi.org/10.1007/s10750-004-4872-5.
Hyde, K.D., Jencso, K., Wilcox, A.C., Woods, S., 2016. Influences of vegetation disturbance on hydrogeomorphic response following wildfire. Hydrol. Process. 30 (7), 1131–1148.
Janyszek-Sołtysiak, M., Grzelak, M., Gajewski, P., Jagodziński, A.M., Gaweł, E., Wrońska-Pilarek, D., 2021. Mineral contents in aboveground biomass of sedges (*Carex* L., Cyperaceae). Energies 14 (23). https://doi.org/10.3390/en14238007. Article 23.
Ji, P., Chen, J., Zhou, A., Ma, R., Chen, R., Chen, S., Lv, F., Ding, G., Liu, Y., Chen, F., 2021. Biofuels reserve controlled wildfire regimes since the last deglaciation: a record from Gonghai Lake, North China. Geophys. Res. Lett. 48 (16), e2021GL094042.
Jia, Q., Li, T., Xiong, Z., Steinke, S., Jiang, F., Chang, F., Qin, B., 2018. Hydrological variability in the western tropical Pacific over the past 700kyr and its linkage to Northern Hemisphere climatic change. Palaeogeogr. Palaeoclimatol. Palaeoecol. 493, 44–54. https://doi.org/10.1016/j.palaeo.2017.12.039.
Johnson, B.G., Johnson, D.W., Chambers, J.C., Blank, R.R., 2011. Fire effects on the mobilization and uptake of nitrogen by cheatgrass (*Bromus tectorum* L.). Plant Soil 341 (1), 437–445. https://doi.org/10.1007/s11104-010-0656-z.
Jolly, W.M., Cochrane, M.A., Freeborn, P.H., Holden, Z.A., Brown, T.J., Williamson, G.J., Bowman, D.M., 2015. Climate-induced variations in global wildfire danger from 1979 to 2013. Nat. Commun. 6 (1), 7537.
Keeley, J.E., 2009. Fire intensity, fire severity and burn severity: a brief review and suggested usage. Int. J. Wildland Fire 18 (1), 116–126.
Keeley, J.E., Syphard, A.D., 2018. Historical patterns of wildfire ignition sources in California ecosystems. Int. J. Wildland Fire 27 (12), 781–799.
Kitzberger, T., Swetnam, T.W., Veblen, T.T., 2001. Inter-hemispheric synchrony of forest fires and the El niño-southern oscillation. Global Ecol. Biogeogr. 10 (3), 315–326.
Klenner, W., Walton, R., Arsenault, A., Kremsater, L., 2008. Dry forests in the Southern Interior of British Columbia: historic disturbances and implications for restoration and management. For. Ecol. Manag. 256 (10), 1711–1722.
Kohn, M.J., 2010. Carbon isotope compositions of terrestrial C3 plants as indicators of (paleo) ecology and (paleo) climate. Proc. Natl. Acad. Sci. USA 107 (46), 19691–19695.
Kokkonen, N.A., Laine, A.M., Laine, J., Vasander, H., Kurki, K., Gong, J., Tuittila, E., 2019. Responses of peatland vegetation to 15-year water level drawdown as mediated by fertility level. J. Veg. Sci. 30 (6), 1206–1216.
Krause, A., Kloster, S., Wilkenskjeld, S., Paeth, H., 2014. The sensitivity of global wildfires to simulated past, present, and future lightning frequency. J. Geophys. Res.: Biogeosciences 119 (3), 312–322.
Kreye, J.K., Kane, J.M., Varner, J.M., Hiers, J.K., 2020. Radiant heating rapidly increases litter flammability through impacts on fuel moisture. Fire Ecol 16, 8. https://doi.org/10.1186/s42408-020-0067-3.
Kuo, N., Ho, C., 2004. ENSO effect on the sea surface wind and sea surface temperature in the Taiwan Strait. Geophys. Res. Lett. 31 (13).
Laiho, R., Vasander, H., Penttilä, T., Laine, J., 2003. Dynamics of plant-mediated organic matter and nutrient cycling following water-level drawdown in boreal peatlands. Global Biogeochem. Cycles 17 (2), 2002GB002015. https://doi.org/10.1029/2002GB002015.
Larridon, I., Reynders, M., Huygh, W., Bauters, K., Van de Putte, K., Muasya, A.M., Boeckx, P., Simpson, D.A., Vrijdaghs, A., Goetghebeur, P., 2011. Affinities in C3 *Cyperus* lineages (Cyperaceae) revealed using molecular phylogenetic data and carbon isotope analysis. Bot. J. Linn. Soc. 167 (1), 19–46.
Larson, D.L., 1995. Effects of climate on numbers of northern prairie wetlands. Climatic Change 30 (2), 169–180. https://doi.org/10.1007/BF01091840.
Laurance, W.F., 2004. Forest-climate interactions in fragmented tropical landscapes. Phil. Trans. Roy. Soc. Lond. B Biol. Sci. 359 (1443), 345–352.
Leipe, C., Lu, J., Chi, K., 2023. Population dynamics in Taiwan from the Neolithic to early historic periods (5000–100 cal BP): linking cultural developments and environmental change. Archaeological Research in Asia 36, 100482. https://doi.org/10.1016/j.ara.2023.100482.
Letnic, M., Tamayo, B., Dickman, C.R., 2005. The responses of mammals to La-Niña (El-Niño Southern Oscillation)–associated rainfall, predation, and wildfire in central Australia. J. Mammal. 86 (4), 689–703.
Li, H., Liu, F., Luo, P., Chen, X., Chen, J., Huang, Z., Peng, J., Xiao, R., Wu, J., 2019. Stimulation of optimized influent C: N ratios on nitrogen removal in surface flow constructed wetlands: performance and microbial mechanisms. Sci. Total Environ. 694, 133575.
Li, H.-C., Liew, P.-M., Seki, O., Kuo, T.-S., Kawamura, K., Wang, L.-C., Lee, T.-Q., 2013. Paleoclimate variability in central Taiwan during the past 30Kyrs reflected by pollen, δ13CTOC, and n-alkane-δD records in a peat sequence from Toushe Basin. New Global Perspectives on Paleontology, Stratigraphy, Paleoceanography, Paleoclimatology, and Tectonics in the East Asia and Western Pacific 69, 166–176. https://doi.org/10.1016/j.jseaes.2012.12.005.
Li, X., Dodson, J., Zhou, J., Zhou, X., 2009. Increases of population and expansion of rice agriculture in Asia, and anthropogenic methane emissions since 5000 BP. Quat. Int. 202 (1–2), 41–50.
Liew, P.-M., Huang, S.-Y., Kuo, C.-M., 2006. Pollen stratigraphy, vegetation and environment of the last glacial and Holocene—a record from Toushe Basin, central Taiwan. Morphodynamics and Climate in Taiwan since the Late Pleistocene 147 (1), 16–33. https://doi.org/10.1016/j.quaint.2005.09.003.
Liew, P.-M., Wu, M.-H., Lee, C.-Y., Chang, C.-L., Lee, T.-Q., 2014. Recent 4000 years of climatic trends based on pollen records from lakes and a bog in Taiwan. Quat. Int. 349, 105–112.
Lin, T.-W., Kaboth-Bahr, S., Bahr, A., Yamoah, K.A., Su, C.-C., Wang, L.-C., Wang, P.-L., Löwemark, L., 2023. Disentangling the impact of anthropogenic and natural processes on the environment in a subtropical subalpine lake catchment in northeastern Taiwan over the past 150 years. Sci. Total Environ. 866, 161300 https://doi.org/10.1016/j.scitotenv.2022.161300.
Littell, J.S., Peterson, D.L., Riley, K.L., Liu, Y., Luce, C.H., 2016. A review of the relationships between drought and forest fire in the United States. Global Change Biol. 22 (7), 2353–2369.
Liu, H., Xu, C., Allen, C.D., Hartmann, H., Wei, X., Yakir, D., Wu, X., Yu, P., 2022. Nature-based framework for sustainable afforestation in global drylands under changing climate. Global Change Biol. 28 (7), 2202–2220. https://doi.org/10.1111/gcb.16059.
Liu, Q., Liu, J., Liu, H., Liang, L., Cai, Y., Wang, X., Li, C., 2020. Vegetation dynamics under water-level fluctuations: implications for wetland restoration. J. Hydrol. 581, 124418.
Liu, Y., Stanturf, J., Goodrick, S., 2010. Trends in global wildfire potential in a changing climate. For. Ecol. Manag. 259 (4), 685–697.
Lloret, F., Calvo, E., Pons, X., Díaz-Delgado, R., 2002. Wildfires and landscape patterns in the eastern iberian peninsula. Landsc. Ecol. 17 (8), 745–759. https://doi.org/10.1023/A:1022966930861.
Magerl, A., Gingrich, S., Matej, S., Cunfer, G., Forrest, M., Lauk, C., Schlaffer, S., Weidinger, F., Yuskiw, C., Erb, K., 2023. The role of wildfires in the interplay of forest carbon stocks and wood harvest in the contiguous United States during the 20th century. Global Biogeochem. Cycles, e2023GB007813.
Malamud-Roam, F., Ingram, B.L., 2004. Late Holocene δ13C and pollen records of paleosalinity from tidal marshes in the San Francisco Bay estuary, California. Quat. Res. 62 (2), 134–145.
Matthias, I., Semmler, M.S.S., Giesecke, T., 2015. Pollen diversity captures landscape structure and diversity. J. Ecol. 103, 880–890.
Maynard, T., 2013. Fire Interactions and Pulsation-Theoretical and Physical Modeling. University of California, Riverside. *Doctoral dissertation*.
McCutchan, M.H., Fox, D.G., 1986. Effect of elevation and aspect on wind, temperature and humidity. J. Appl. Meteorol. Climatol. 25 (12), 1996–2013.
McGlinn, D., Xiao, X., McGill, B., May, F., Engel, T., Oliver, C., Blowes, S., Knight, T., Purschke, O., Gotelli, N., Chase, J., 2021. mobr: Measurement of Biodiversity, 2.0.2) [R-Packages]. https://cran.r-project.org/web/packages/mobr/index.html.
Meigs, G.W., Dunn, C.J., Parks, S.A., Krawchuk, M.A., 2020. Influence of topography and fuels on fire refugia probability under varying fire weather conditions in forests of the Pacific Northwest, USA. Can. J. For. Res. 50 (7), 636–647.
Meyers, P.A., 1997. Organic geochemical proxies of paleoceanographic, paleolimnologic, and paleoclimatic processes. Org. Geochem. 27 (5–6), 213–250.
Meyers, P.A., 2003. Applications of organic geochemistry to paleolimnological reconstructions: a summary of examples from the Laurentian Great Lakes. Org. Geochem. 34 (2), 261–289.
Oksanen, J., Simpson, G.L., Blanchet, F.G., Kindt, R., Legendre, P., Minchin, P.R., O'Hara, R.B., Solymos, P., Stevens, M.H.H., Szoecs, E., Wagner, H., Barbour, M., Bedward, M., Bolker, B., Borcard, D., Carvalho, G., Chirico, M., Caceres, M.D., Durand, S., Weedon, J., 2022. vegan: Community Ecology Package (2.6-4) [R-Packages]. https://cran.r-project.org/web/packages/vegan/index.html.
Page, S., Hoscilo, A., Langner, A., Tansey, K., Siegert, F., Limin, S., Rieley, J., 2009. Tropical peatland fires in southeast Asia. In: Cochrane, M.A. (Ed.), Tropical Fire

Ecology. Springer Berlin Heidelberg, pp. 263–287. https://doi.org/10.1007/978-3-540-77381-8_9.
Pang, Y., Zhou, B., Zhou, X., Xu, X., Liu, X., Zhan, T., Lu, Y., 2021. Abundance and δ13C of sedimentary black carbon indicate rising wildfire and C4 plants in Northeast China during the early Holocene. Palaeogeogr. Palaeoclimatol. Palaeoecol. 562, 110075.
Pausas, J.G., Keeley, J.E., 2021. Wildfires and global change. Front. Ecol. Environ. 19 (7), 387–395. https://doi.org/10.1002/fee.2359.
Pezeshki, S.R., 2001. Wetland plant responses to soil flooding. Environ. Exp. Bot. 46 (3), 299–312.
Popović, Z., Bojović, S., Marković, M., Cerdà, A., 2021. Tree species flammability based on plant traits: a synthesis. Sci. Total Environ. 800, 149625 https://doi.org/10.1016/j.scitotenv.2021.149625.
Potera, C., 2009. Climate Change: Challenges of Predicting Wildfire Activity.
Prichard, S.J., Stevens-Rumann, C.S., Hessburg, P.F., 2017. Tamm Review: shifting global fire regimes: lessons from reburns and research needs. For. Ecol. Manag. 396, 217–233. https://doi.org/10.1016/j.foreco.2017.03.035.
Rahman, A., Chang, W.-C., Kashima, K., Fukumoto, Y., Huang, J.-J.S., Löwemark, L., Wang, L.-C., Chang, Y.-P., 2024. Late Holocene paleoclimate reconstruction of northern Taiwan using a multiproxy approach in the Dream Lake sediment core. Quat. Int.
Rahman, A., Rathi, A., Nambiar, R., Mishra, P.K., Anoop, A., Bhushan, R., Kumar, S., 2021. Signatures of natural to anthropogenic transition in lake sediments from the Central Himalaya using stable isotopes. Appl. Geochem. 134, 105095.
Rahman, A., Sarkar, S., Kumar, S., 2020. Paleoenvironment of the Central Himalaya during late MIS 3 using stable isotopic compositions of lacustrine organic matter occluded in diatoms and sediments. Quat. Int. 558, 1–9.
Rajagopalan, G., Ramesh, R., Sukumar, R., 1999. Climatic implications of δ13C and δ18O ratios from C3 and C4 plants growing in a tropical montane habitat in southern India. J. Biosci. 24 (4), 491–498. https://doi.org/10.1007/BF02942661.
Reimer, P.J., Austin, W.E., Bard, E., Bayliss, A., Blackwell, P.G., Ramsey, C.B., Butzin, M., Cheng, H., Edwards, R.L., Friedrich, M., 2020. The IntCal20 Northern Hemisphere radiocarbon age calibration curve (0–55 cal kBP). Radiocarbon 62 (4), 725–757.
Remy, C.C., Magne, G., Stivrins, N., Aakala, T., Asselin, H., Seppä, H., Luoto, T., Jasiunas, N., Ali, A.A., 2023. Climatic and vegetational controls of Holocene wildfire regimes in the boreal forest of northern Fennoscandia. J. Ecol. 111 (4), 845–860.
Ren, L., Ji, J., Wang, Y., Bu, S., Lu, Z., Luo, X., 2022. Investigation into spatiotemporal characteristics of coastal winds around the Taiwan Island. Energy Rep. 8, 419–427.
Rogers, B.M., Soja, A.J., Goulden, M.L., Randerson, J.T., 2015. Influence of tree species on continental differences in boreal fires and climate feedbacks. Nat. Geosci. 8 (3), 228–234.
Rossa, C.G., Veloso, R., Fernandes, P.M., 2016. A laboratory-based quantification of the effect of live fuel moisture content on fire spread rate. Int. J. Wildland Fire 25 (5), 569–573.
Ruffault, J., Curt, T., Martin-StPaul, N.K., Moron, V., Trigo, R.M., 2018. Extreme wildfire events are linked to global-change-type droughts in the northern Mediterranean. Nat. Hazards Earth Syst. Sci. 18 (3), 847–856.
Seidl, R., Schelhaas, M., Lexer, M.J., 2011. Unraveling the drivers of intensifying forest disturbance regimes in Europe. Global Change Biol. 17 (9), 2842–2852.
Shah, R.A., Achyuthan, H., Lone, A.M., Kumar, S., Kumar, P., Sharma, R., Amir, M., Singh, A.K., Dash, C., 2020. Holocene palaeoenvironmental records from the high-altitude Wular Lake, western himalayas. Holocene 30 (5), 733–743. https://doi.org/10.1177/0959683619895592.
Shah, R.A., Khan, I., Rahman, A., Kumar, S., Achyuthan, H., Shukla, A.D., Kumar, P., Dash, C., 2022. Holocene climate events and associated land use changes in the eastern coast of India: inferences from the Chilika Lagoon. Holocene 32 (10), 1081–1090.
Shah, R.A., Rahman, A., Yadava, M.G., Kumar, S., 2023. Mid–late Holocene palaeoclimate and biogeochemical evolution of Wular Lake, Kashmir valley, India. J. Quat. Sci. (n/a) https://doi.org/10.1002/jqs.3565. *n/a*.
Stephens, S.L., Collins, B.M., Fettig, C.J., Finney, M.A., Hoffman, C.M., Knapp, E.E., North, M.P., Safford, H., Wayman, R.B., 2018. Drought, tree mortality, and wildfire in forests adapted to frequent fire. Bioscience 68 (2), 77–88.
Stevens, A., Ramirez-Lopez, L., Hans, G., 2022. Prospectr: Miscellaneous Functions for Processing and Sample Selection of Spectroscopic Data (0.2.6) [R-Packages]. https://cran.r-project.org/web/packages/prospectr/index.html.
Syphard, A.D., Keeley, J.E., 2015. Location, timing and extent of wildfire vary by cause of ignition. Int. J. Wildland Fire 24 (1), 37–47.
Tan, Z., Han, Y., Cao, J., Huang, C.C., An, Z., 2015. Holocene wildfire history and human activity from high-resolution charcoal and elemental black carbon records in the Guanzhong Basin of the Loess Plateau, China. Quat. Sci. Rev. 109, 76–87.
Tan, Z., Huang, C.C., Pang, J., Zhou, Y., 2013. Wildfire history and climatic change in the semi-arid loess tableland in the middle reaches of the Yellow River of China during the Holocene: evidence from charcoal records. Holocene 23 (10), 1466–1476.
Tao, T., 2024. Climate Trends and Anomalies and Their Impact on Forest Fire Size and Frequency from 1986 to 2020 in Canada. University of Alberta. Doctoral dissertation.
Thompson, R., Battarbee, R.W., O'Sullivan, P.E., Oldfield, F., 1975. Magnetic susceptibility of lake sediments. Limnol. Oceanogr. 20 (5), 687–698. https://doi.org/10.4319/lo.1975.20.5.0687.
Tieszen, L.L., Senyimba, M.M., Imbamba, S.K., Troughton, J.H., 1979. The distribution of C3 and C4 grasses and carbon isotope discrimination along an altitudinal and moisture gradient in Kenya. Oecologia 37 (3), 337–350. https://doi.org/10.1007/BF00347910.
Touchette, B.W., Frank, A., Iannacone, L.R., Turner, G., 2008. Drought susceptibility in emergent wetland angiosperms: a comparison of water deficit growth in five herbaceous perennials. Wetl. Ecol. Manag. 16 (6), 485–497. https://doi.org/10.1007/s11273-008-9086-6.
Tumino, B.J., Duff, T.J., Goodger, J.Q.D., Cawson, J.G., 2019. Plant traits linked to field-scale flammability metrics in prescribed burns in *Eucalyptus* forest. PLoS One 14 (8), e0221403. https://doi.org/10.1371/journal.pone.0221403.
Vachula, R.S., Richter, N., 2018. Informing sedimentary charcoal-based fire reconstructions with a kinematic transport model. Holocene 28 (1), 173–178.
Vamvuka, D., Sfakiotakis, S., 2011. Combustion behaviour of biomass fuels and their blends with lignite. Thermochim. Acta 526 (1–2), 192–199.
Varner, J.M., Kane, J.M., Kreye, J.K., Engber, E., 2015. The flammability of forest and woodland litter: a synthesis. Curr. For. Rep. 1, 91–99. https://doi.org/10.1007/s40725-015-0012-x.
Verma, S., Rahman, A., Shah, R.A., Agrawal, R.K., Yadava, M., Kumar, S., 2023. Late Holocene fire and precipitation history of the Kashmir Himalaya: inferences from black carbon in lake sediments. Palaeogeogr. Palaeoclimatol. Palaeoecol., 111401
Villarreal, M.L., Norman, L.M., Yao, E.H., Conrad, C.R., 2022. Wildfire probability models calibrated using past human and lightning ignition patterns can inform mitigation of post-fire hydrologic hazards. Geomatics, Nat. Hazards Risk 13 (1), 568–590. https://doi.org/10.1080/19475705.2022.2039787.
Walker, R.B., Coop, J.D., Parks, S.A., Trader, L., 2018. Fire regimes approaching historic norms reduce wildfire-facilitated conversion from forest to non-forest. Ecosphere 9 (4), e02182.
Wang, G.G., Kemball, K.J., 2005. Effects of fire severity on early development of understory vegetation. Can. J. For. Res. 35 (2), 254–262.
Wang, L.-C., 2021. Using paleoecological data to inform the conservation strategy for floristic diversity and *Isoetes taiwanensis* in northern taiwan. Diversity 13 (8). https://doi.org/10.3390/d13080395.
Wang, L.-C., 2024. Subtropical montane vegetation dynamics in response to Holocene climate change in central Taiwan. Veg. Hist. Archaeobotany. https://doi.org/10.1007/s00334-024-00988-8.
Wang, L.-C., Behling, H., Kao, S.-J., Li, H.-C., Selvaraj, K., Hsieh, M.-L., Chang, Y.-P., 2015. Late Holocene environment of subalpine northeastern Taiwan from pollen and diatom analysis of lake sediments. J. Asian Earth Sci. 114, 447–456. https://doi.org/10.1016/j.jseaes.2015.03.037.
Wang, L.-C., Chang, Y.-P., Li, H.-C., Chen, S.-H., Wu, J.-T., Lee, T.-Q., Shiau, L.-J., 2020. Revealing the vegetation, fire and human activities in the lowland of eastern Taiwan during Late Holocene. Quat. Int. 544 (10), 32–40. https://doi.org/10.1016/j.quaint.2018.08.003.
Wang, L.-C., Tang, Z.-W., Chen, H.-F., Li, H.-C., Shiau, L.-J., Huang, J.-J.S., Wei, K.-Y., Chuang, C.-K., Chou, Y.-M., 2019. Late Holocene vegetation, climate, and natural disturbance records from an alpine pond in central Taiwan. Quat. Int. 528, 63–72. https://doi.org/10.1016/j.quaint.2019.03.005.
Wara, M.W., Ravelo, A.C., Delaney, M.L., 2005. Permanent El niño-like conditions during the pliocene warm period. Science 309 (5735), 758–761. https://doi.org/10.1126/science.1112596.
Ward, D.E., Hardy, C.C., 1991. Smoke emissions from wildland fires. Environ. Int. 17 (2–3), 117–134.
Wei, T., Simko, V., Levy, M., Xie, Y., Jin, Y., Zemla, J., Freidank, M., Cai, J., Protivinsky, T., 2021. *Corrplot: Visualization Of a Correlation Matrix* (0.92). R-Packages; R-Packages. https://cran.r-project.org/web/packages/corrplot/index.html.
Wenske, D., Böse, M., Frechen, M., Lüthgens, C., 2011. Late Holocene mobilisation of loess-like sediments in Hohuan Shan, high mountains of Taiwan. Quat. Int. 234 (1–2), 174–181.
Whitlock, C., Larsen, C., 2001. Charcoal as a fire proxy. Tracking Environmental Change Using Lake Sediments: Terrestrial, Algal, and Siliceous Indicators 75–97.
Whitlock, C., Larsen, C., 2002. Charcoal as a fire proxy. In: Smol, J.P., Birks, H.J.B., Last, W.M., Bradley, R.S., Alverson, K. (Eds.), Tracking Environmental Change Using Lake Sediments, vol. 3. Kluwer Academic Publishers, pp. 75–97. http://www.springerlink.com/content/l84138365qt56243/.
Wu, I.C., 2009. Photosynthetic Pathway, Ecological Characteristics and Geographical Distribution of Cyperoidaea in Taiwan. National Chung Keng University. M.Sc.
Yedinak, K.M., Strand, E.K., Hiers, J.K., Varner, J.M., 2018. Embracing complexity to advance the science of wildland fire behavior. Fire 1 (2), 20.
Yoshida, S., Morimoto, T., Ushio, T., Kawasaki, Z., 2007. ENSO and convective activities in Southeast Asia and western Pacific. Geophys. Res. Lett. 34. https://doi.org/10.1029/2007GL030758.
Yuan, Z., Wu, D., Wang, T., Ma, X., Li, Y., Shao, S., Zhang, Y., Zhou, A., 2022. Holocene fire history in southwestern China linked to climate change and human activities. Quat. Sci. Rev. 289, 107615.
Zhang, Y., Cui, Q., Blockley, S., Zhou, A., Chen, L., Boyall, L., Colombaroli, D., 2023. Fire history in the qinling mountains of east-Central China since the last glacial maximum. Geophys. Res. Lett. 50 (10), e2023GL102848 https://doi.org/10.1029/2023GL102848.
Zhong, Y., Jiang, M., Middleton, B.A., 2020. Effects of water level alteration on carbon cycling in peatlands. Ecosys. Health Sustain. 6 (1), 1806113 https://doi.org/10.1080/20964129.2020.1806113.
Zumbrunnen, T., Bugmann, H., Conedera, M., Bürgi, M., 2009. Linking forest fire regimes and climate—a historical analysis in a dry inner alpine valley. Ecosystems 12 (1), 73–86. https://doi.org/10.1007/s10021-008-9207-3.